

Stellar Orbits Around the Galactic Center Black Hole

A. M. Ghez¹, S. Salim, S. D. Hornstein, A. Tanner, M. Morris, E. E. Becklin, G. Duchêne

UCLA Division of Astronomy and Astrophysics, Los Angeles, CA 90095-1562

ghez, samir, seth, tanner, morris, becklin, duchene@astro.ucla.edu

ABSTRACT

We present new diffraction-limited images of the Galactic Center, obtained with the W. M. Keck I 10-meter telescope. Within $0''.4$ of the Galaxy's central dark mass, 22 proper motion stars, with K magnitudes ranging from 13.9 to 17.7, are identified and 15 of these are new detections. In this sample, three newly identified (S0-16, S0-19, and S0-20) and five previously known (S0-1, S0-2, S0-3, S0-4, and S0-5) sources have measured proper motions that reveal orbital solutions.

Orbits are derived *simultaneously* so that they jointly constrain the central dark object's properties: its mass, its position and, for the first time using orbits, its motion on the plane of the sky. This analysis pinpoints the Galaxy's central dark mass to within 1.5 milli-arcsec (mas) and limits its proper motion to 0.8 ± 0.7 mas y^{-1} with respect to central stellar cluster. This localization of the central dark mass is consistent with our derivation of the position of the radio source Sgr A* in the infrared reference frame (± 7 mas), but with an uncertainty that is a factor 5 times smaller, which greatly facilitates searches for near infrared counterparts to the central black hole. Consequently, it now appears that the candidate counterpart to Sgr A* proposed by Genzel et al. (1997) was simply a 1996 detection of the fast moving star S0-19, which, at that time, was close to periape. The estimated central dark mass from orbital motions is $(4.0 \pm 0.3) \times 10^6 (\frac{R_0}{8kpc})^3 M_\odot$; this is a more direct measure of mass than those obtained from velocity dispersion measurements, which are as much as a factor of two smaller, and makes, for the first time, the Galactic center's distance, which adds an additional 19% uncertainty in the estimated mass, the limiting source of uncertainty in the absolute mass. For stars in this sample, the closest approach is achieved by S0-16, which confines the mass to within a radius of a mere 90 AU ($= 0.0004$ pc $= 12$ light-hours $= 1,000 R_{sh}$) and increases the inferred dark

¹Institute of Geophysics and Planetary Physics, University of California, Los Angeles, CA 90095-1565

mass density by four orders of magnitude compared to earlier analyses based on velocity and acceleration vectors, making the Milky Way the strongest existing case for a supermassive black hole at the center of any normal type galaxy.

With well determined orbital parameters for 8 stars, the dynamical properties of the central stellar cluster can now be studied directly. While the distributions of eccentricities, after correcting for selection effects, and the directions of the angular momentum vectors are consistent with those of an isotropic system, the distribution of the apoapse directions is not, at the 2σ level. Furthermore, there appears to be an inner cutoff in the distribution of apoapse distances for stars brighter than $K \sim 15.5$, with a minimum value of ~ 1800 AU. Nonetheless, the apoapse distances are remarkably small in light of the spectroscopic identification of the majority of these stars as having hot photospheres consistent with massive, young stars (< 10 Myr). Unfortunately, the existing theories that produce young stars, or old stars that look young, in close proximity to a central supermassive black hole are all somewhat problematic. However, if the bias in the distribution of apoapse directions is real, this would favor a formation scenario in which the Sgr A* cluster stars are young stars that have been tidally stripped from a dense inspiraling cluster near the cluster's periapse passage ($\lesssim 1800$ AU) and subsequently scattered inward. Understanding the apparent youth of stars in the Sgr A* cluster, as well as the more distant He I emission line stars, has now become one of the major outstanding issues in the study of the Galactic Center.

Subject headings: black hole physics – Galaxy:center — Galaxy:kinematics and dynamics — infrared:stars – techniques:high angular resolution

1. Introduction

The proximity of our Galaxy's center (8 kpc, Reid 1993) presents an opportunity to build a case for a supermassive black hole and to study the black hole's environment and its effects thereon with much higher spatial resolution than can be brought to bear on any other galaxy. The first hint of a central concentration of dark matter in the Milky Way came from radial velocity measurements of ionized gas located in a three-armed structure known as the mini-spiral, which extends from the center out to ~ 1 -2 pc (Lacy et al. 1980). Concerns that the measured gas motions were not tracing the gravitational potential were quickly allayed by radial velocity measurements of stars, which are not susceptible to non-gravitational forces (McGinn et al. 1989; Sellgren et al. 1990; Haller et al. 1996; Genzel et al. 1997). These early, low angular resolution, dynamical measurements of the gas and

stars at the center of the Milky Way suggested the presence of $\sim 3 \times 10^6 M_\odot$ of dark matter and confined it to within a radius of ~ 0.1 pc. The implied minimum dark matter density of $\sim 3 \times 10^9 M_\odot/pc^3$, however, still allowed a cluster of dark objects, such as neutron stars or stellar mass black holes, as one of the alternatives to a single supermassive black hole, because the measurements did not force the cluster’s lifetime to be shorter than the age of the Galaxy (Maoz et al. 1998).

Significant progress has been made recently with diffraction-limited near-infrared studies of the central stellar cluster. The first phase of these experiments yielded proper motion velocities (Eckart & Genzel 1997; Ghez et al. 1998), which suggested that $(2.6 \pm 0.6) \times 10^6 M_\odot$ of dark matter is confined to within 0.015 pc. This increased the implied minimum dark matter density by 3 orders of magnitude to $10^{12} M_\odot/pc^3$ and eliminated a cluster of dark objects as a possible explanation of the Galaxy’s central dark mass concentration (Maoz et al. 1998), but still left the fermion ball hypothesis (e.g., Tsiklauri & Viollier 1998, Munyaneza & Viollier 2002) as an alternative to a single supermassive black hole. The velocity dispersion measurements also localized the dark matter’s centroid to within 100 mas and at a position consistent with the nominal location of the unusual radio source Sgr A* (Ghez et al. 1998), whose emission is posited to arise from accretion onto a central supermassive black hole (e.g., Lo et al. 1985). The detection of acceleration for three stars – S0-1, S0-2, and S0-4 – originating from the same center, localized the dark mass to within 30 mas, increased the dark matter’s minimum density to $10^{13} M_\odot/pc^3$, and thereby further strengthened both the case for a supermassive black hole and its association with Sgr A* (Ghez et al. 2000; Eckart et al. 2002).

Deviations from linear motions also initiated a new phase for these proper motion experiments, that of direct orbital studies. By making a number of assumptions, including fixing the central mass to the value obtained from the velocity dispersion analysis and its location to that inferred for Sgr A* by Menten et al. (1997), Ghez et al. (2000) and Eckart et al. (2002) obtained first crude orbital solutions; these experiments revealed that orbital periods for S0-2 and S0-1 could be as short as 15 and 35 years, respectively. With more of the orbit being traced, more precise orbital analyses have been carried out for S0-2 by Schödel et al. (2002), who dropped the mass assumption, and by Ghez et al. (2003), who dropped both the mass and center of attraction assumptions and added radial velocity measurements. These orbital solutions suggested S0-2 made a closest approach of 0.0006 pc (120 AU) in 2002 and is estimated to enclose a central mass of $(3.7 \pm 1.5) \times 10^6 M_\odot$ by Schödel et al. (2002) and $(4.0 \pm 0.6) \times 10^6 M_\odot$ by Ghez et al. (2003)², which is higher than that found

²The uncertainties in the estimated mass in Ghez et al. (2003) are a factor of 2.5 smaller than that in Schödel et al. (2002), despite the two additional free model parameters introduced by fitting for the center

from the velocity dispersion measurements. Possible causes of this discrepancy include (1) inaccuracies in the assumptions made in the use of the velocity-dispersion-based projected mass estimators about the stellar cluster’s number density distribution and/or the level of anisotropy (Genzel et al. 2000), (2) inaccuracies in the orbital fit assumptions, such as the central mass distribution being point-like and at rest with respect to the central stellar cluster, and (3) systematic errors in either the overall velocity dispersion measurement for the central stellar cluster or S0-2’s individual positional measurements. Further measurements are necessary to determine the origin of the difference in the estimates of the central dark mass produced by the two methods.

While the detection of spectral lines in S0-2 provided full dynamical information, it also offered insight into the nature of this star that is orbiting in such close proximity to the central dark mass. S0-2’s spectral features are consistent with those of an O8-B0 dwarf, suggesting that it is a massive ($\sim 15 M_{\odot}$), young (< 10 Myr), main sequence star (Ghez et al. 2003). Less direct measurements of other stars within the central $1'' \times 1''$, which are known collectively as the Sgr A* stellar cluster, imply that these stars might be similarly young; specifically, their similar $2 \mu\text{m}$ luminosities and the lack of CO absorption in spectra of individual stars (Genzel et al. 1997; Gezari et al. 2002) or in integrated spectra of the Sgr A* stellar cluster (Eckart, Ott, & Genzel 1999; Figer et al. 2000) lead one to conclude that they, like S0-2, have hot photospheres consistent with massive young stars.

While the presence of young stars in close proximity to the Galactic black hole has long been recognized as a problem in the context of the young He I emission line stars (Sanders 1992, Morris 1993), this problem is much worse for the Sgr A* cluster stars, whose distances from the black hole are an order of magnitude smaller. At S0-2’s apoapse distance of 0.01 pc, inferred from the orbital solutions, the Roche density is 10^{14} cm^{-3} , whereas the maximum density determined for even the nearby circumnuclear disk, located at radii of $\sim 1\text{-}3$ pc, is only about 10^5 cm^{-3} (e.g., Jackson et al. 1993). Furthermore, at present, the region over which S0-2 is currently orbiting contains only a very low-density plasma, as evidenced by weak Br- γ line emission (Figer et al. 2000; Gezari et al. 2002). Several ideas proposed to account for the apparently young He I emission line stars may be applicable to the Sgr A* cluster stars; they fall broadly into the two categories of “nature”, in which case star formation did indeed occur very recently, and “nurture”, in which case the extreme environment at the Galactic center has significantly altered the evolution of these stars. Stellar kinematics produced by these mechanisms are likely to differ. Well constrained orbits for multiple stars in the Sgr A* cluster would allow a direct examination of the cluster’s

of attraction and the shorter time baseline. This is primarily due to the higher astrometric accuracy of the Keck data set, rather than the inclusion of radial velocity measurements.

kinematics and therefore would provide important insight into how these stars formed and came to be on their present orbits.

This paper reports new proper motion measurements obtained with the W. M. Keck 10-meter telescope for 5 previously known stars (S0-1, S0-2, S0-3, S0-4, S0-5) and for 3 newly identified stars (S0-16, S0-19, S0-20). The trajectories of all of these stars show significant curvature or linear acceleration, thus allowing the first *simultaneous* orbital analysis for multiple stars making their closest approaches to the central dark mass. Section 2 describes the observations, which now cover an 8 year time baseline. Section 3 provides the details and results for source identification, astrometry, and the orbital fits, which, for the first time, allows for the dark mass’ motion on the plane of the sky. Finally, Section 4.1 discusses the constraints that the orbital parameters offer on the nature of the central dark mass distribution, which has become the best case yet for a supermassive black hole at the center of any normal type galaxy and whose mass, position and motion in the infrared reference frame are determined with unprecedented accuracy, and Section 4.2 explores how the direct measurements of orbital dynamics impacts the question of origin of the central stellar cluster.

2. Observations

New $K[2.2 \mu m]$ -band speckle imaging observations of the Galaxy’s central stellar cluster were obtained with the W. M Keck I 10-meter telescope using the facility near-infrared camera, NIRC (Matthews & Soifer 1994; Matthews et al. 1996) on the nights of 2000 April 21, 2000 May 19-20, 2000 July 19-20, 2000 Oct 18, 2001 May 7-9, 2001 July 28-29, 2002 April 23-24, 2002 May 23-24 & 28-29, 2002 June 2, 2002 July 19-20, and 2003 April 21-22. These data sets were collected and analyzed similarly to the data sets obtained between 1995 and 1999 for this project (see Ghez et al. 1998, 2000 for details). In summary, short ($t_{exp} = 0.1$ sec) exposures were obtained in sets of ~ 200 , resulting in a total of $\sim 10,000$ exposures per observing run. Each frame, with a scale of 20.456 ± 0.027 mas/pixel (see Appendix B) and a corresponding field of view of $5.22'' \times 5.22''$, was sky-subtracted, flat fielded, bad pixel-corrected, corrected for distortion effects, and magnified by a factor of two. In sets of 200, the frames were shifted to the location of the brightest speckle of IRS 16C and combined to create intermediate shift-and-add (SAA) maps, which have point spread functions (PSF) that can be described as containing a diffraction-limited core on top of a seeing halo. These were then combined after applying a seeing cut, which required that the seeing halos be below a value that optimized the detection of point sources in a crowded field - typically $< 0.''6$. In addition to averaging all the data from each run to produce a final SAA map, these data were divided into three sub-sets to construct “sub-maps”, which were used to

determine positional and brightness uncertainties.

3. Data Analysis & Results

3.1. Source Identification

Sources are identified using the same procedure described by Ghez et al. (1998), with three modifications. In this approach, a “match filter” is applied to each image, by cross-correlating the image with the core of its PSF, out to a radius of $0.''06$ (see Figure 1). In a first pass at source identification, correlation peaks larger than a threshold value are flagged as stars. Once stars are identified, a second lower threshold value is used to track these stars in images in which they were not identified with the first threshold value; this second pass search is limited to within some radius of the predicted position. While in Ghez et al. (1998) the predicted position was simply the position found in the first pass, here we use any kinematic information available from the first pass to define this predicted position. The other two modifications change only the values used in the algorithm. We lowered the first pass threshold correlation value for source identification from 0.7 to 0.5, which allows fainter sources to be identified, and we have decreased the second pass search area radius from $0.''7$ to $0.''5$, due to the increased number of sources that are being tracked. While many sources are identified and tracked over our entire $\sim 5'' \times 5''$ field of view, this study is limited to sources within a radius of $0.''4$ of the infrared position for Sgr A* (see Appendix B); the radius is set by the criteria that all stars with accelerations of 2 mas y^{-2} or greater should reside within this region, assuming a mass, M , of $4 \times 10^6 M_\odot$, or equivalently $r_{max}^2 = GM/a_{min}$.

This procedure identifies 22 sources, of which 15 are newly discovered in this study. As can be seen in Figure 1, which labels all the sources, the source identification approach used here is still fairly conservative and a number of additional sources are seen in the cross-correlation maps. The new sources are named according to the convention introduced in Ghez et al. 1998 and summarized in Appendix A. Table 1 lists the properties of all the detected sources. The average magnitudes reveal that the new sources are all fainter than the sources in this study that were previously published ($K \gtrsim 15.1 \text{ mag}$).³ While the previously known sources are detected in all the maps, the new sources are not, due to the variation in the maps’ sensitivities and, occasionally, confusion with a brighter source; for instance, S0-16

³Among the original proper motion sample reported in Ghez et al (1998), there are sources comparably faint to the newly discovered proper motion sources, but at larger radii; the reason for this is that at the center of the maps source confusion lowers the correlation values and reduces the sensitivity to faint sources using the source identification technique applied in this study.

and S0-19 are each lost in one year as they passed within $0''.03$ and $0''.02$ of S0-3 and S0-2, respectively. Reliably identifying and tracking stars fainter than $K \sim 15$ mag through such a crowded region required multiple maps per year, which we began to obtain in 1998.

3.2. Astrometry

Stellar astrometry is derived in three separate steps. First, centroid positions on the correlation peaks provide estimates of the stars' locations in each of the maps. These locations are estimated with an accuracy of ~ 0.1 pixels (2 mas) for the brightest star and ~ 0.25 pixels (5 mas) for the $K \sim 15.5$ stars, with uncertainties estimated based on the rms of their locations in the 3 sub-maps created for each map (see §2). Second, the coordinate system for each map is transformed, with the application of a net translation and rotation, to a common local reference frame. As in Ghez et al. (1998), this transformation is determined by minimizing the net motion of the measured stars, but with two modifications. First, rather than using all stars detected in the central $\sim 5'' \times 5''$, we now exclude those stars with velocities greater than 600 km/s. Second, the common local reference frame is now chosen to be the map obtained at the median epoch, 1999 July, instead of the 1995 June map. This method for obtaining the relative positions of stars minimizes uncertainties from the transformation process at the center of the field of view, which is where the stars reported here were always placed. Uncertainties in the transformations to a common coordinate system for the stars in Table 1 are ~ 0.05 - 0.1 pixels (1-2 mas) and are, therefore, negligible compared to positional uncertainties in the original maps for the faintest stars and comparable to that of the brightest stars in our sample. The uncertainties from the centroiding and transformation process are added in quadrature to produce the final relative position uncertainties. It is the relative positions that are used in the orbital analysis presented in §3.3.1. The orbital solutions presented in §3.3.2 have been oriented and scaled with respect to an absolute reference frame using measurement of sources with known absolute astrometry, as described in Appendix B.

3.3. Orbital Analysis

Significant curvature or linear acceleration in the plane of the sky is detected for 8 of the 19 sources listed in Table 1; specifically, S0-1, S0-2, S0-3, S0-4, S0-5, S0-16, S0-19, and S0-20 all have detectable accelerations in the plane of the sky of at least 2 mas y^{-2} and as much as 1500 mas y^{-2} . We therefore carry out simultaneous orbital fits for these stars with a model described in §3.3.1 and with resulting orbital parameters given in §3.3.2.

3.3.1. Model & Method

We assume a model in which the gravitational potential arises from a single dominant point mass, which allows multiple stars to contribute simultaneously to the solution for the following properties of the central object: mass (M), location (r_{RA} , r_{DEC}), and linear motion on the plane of the sky (v_{RA} , v_{DEC}). In this analysis, the point source’s distance (R_o) and its linear motion along the line of sight (v_z) are not solved for; to get M , R_o is assumed to be 8 kpc (Reid 1993), while v_z is set to 0⁴. In addition to these 5 common free parameters, there are the following 6 free parameters for each star: [1] period (P), which, when combined with the estimate of the central dark mass, yields the angular semi-major axis (A), [2] eccentricity (e), [3] time of periape passage (T_o), which is when the star comes closest to the central dark mass, [4] inclination (i), which is the angle between the normal to the orbital plane and the line of sight and has values ranging from 0 to 180°, with values less than 90° corresponding to direct motion (position angles increasing with time) and values greater than 90° corresponding to retrograde motion, [5] position angle of the nodal point (Ω), which is the position angle, measured Eastward of North, of the line of intersection between the plane of the sky through the central dark mass and the orbital plane⁵, and [6] longitude of periape (ω), which is the angle in the plane of the orbit, in the direction of motion, from node to periastron, with permitted values ranging from 0 to 360°. In total, this model contains $5 + N \times 6$ parameters, where N is the number of stars included in the simultaneous fit. This is a more powerful approach than simply averaging the results of N independent orbital analyses, since each star in a simultaneous solution contributes to the determination of the common parameters, which in turn leads to a better definition of each star’s orbital parameters.

The orbital fits, shown in Figure 2, are carried out by minimizing the chi-squared value between the data and the model and the reported uncertainties are obtained from the covariance matrix, which corresponds roughly to changing the total chi-squared values by 1.

⁴Setting v_z equal to 0 km s⁻¹ is reasonable given that the resulting limits on the values of v_{RA} and v_{DEC} (~ 30 km s⁻¹) are comparable to the uncertainties on the radial velocity measurements for S0-2 (~ 40 km s⁻¹, Ghez et al. 2003), which are the only radial velocities available for this analysis. Furthermore, Figer et al. (in prep) find an average v_z for a set of cool stars consistent with 0 to within 11 km s⁻¹.

⁵In the absence of radial velocity measurements (e.g., all stars except S0-2), it is not possible to distinguish between the ascending and descending nodes, which correspond to the nodal points where the star is moving away from and towards us, respectively, and, by convention, the value less than 180° is taken; this ambiguity generates a similar 180° ambiguity in the longitude of periape. With radial velocity measurements (e.g., S0-2, Ghez et al. 2003), these ambiguities are removed and the ascending node is given for Ω , with permitted values ranging from 0 to 360°.

In total, the data set consists of 284 measurements - 141 positional measurements, each of which provides two independent data points (one for the East-West position and the other for the North-South position), and 2 radial velocity measurements of S0-2 from a single year, reported by Ghez et al. (2003). While the final orbital parameters reported in Tables 2 & 3 come from a simultaneous fit, which is described in detail below, we first carried out a number of independent and semi-independent orbital solutions to check the validity of using common values for the central dark mass as well as to check our estimates of the positional uncertainties ⁶. In these preliminary fits, the central dark mass was not allowed to move. The fully independent solutions yield locations for the central dark mass that are consistent to within 3σ , with individual uncertainties of 1.5, 7.0, and 60 mas for S0-2, S0-16 and S0-19, respectively, and larger uncertainties for the remaining stars. Consistency for the central dark mass is checked by carrying out a semi-independent fit in which the central dark object’s location is treated as a common parameter, but its mass is not. This fit is carried out with the 3 stars - S0-2, S0-16, and S0-19 - that yield meaningful independent mass estimates ($M/\delta M > 3$), which are consistent to within 2σ , with uncertainties of 0.6, 0.6, 0.8 ($\times 10^6$) M_\odot , respectively. It therefore appears to be well justified to simultaneously fit the data with a model in which the central dark object’s properties (M , r_{RA} , r_{DEC} , v_{RA} , and v_{DEC}) are common to all the stars. Using an algorithm described by Salim & Gould (1999), we solve for the orbital parameters simultaneously with the inclusion of the central dark object’s linear motion on the plane of the sky as a free parameter. Since S0-2, S0-16, and S0-19 are the only stars that have any significant implications for the central dark object’s properties, we divide the problem into two. A three-star simultaneous fit with S0-2, S0-16, and S0-19 provides the orbital parameters for these three stars as well as the central dark object’s properties. The orbital parameters for each of the remaining stars are obtained from a four-star simultaneous fit, which includes the star in question plus S0-2, S0-16, and S0-19; this was done to appropriately include the effects of the uncertainties in the central dark object’s parameters in estimates of the remaining stars’ orbital parameters. The resulting χ^2_{dof} for all the simultaneous fits are comparable to 1, again supporting the use of a point mass potential model.

⁶We scale all the estimated relative position uncertainties by a scale factor, which produces a χ^2_{dof} of 1 for the best independent fits; these scale factors modify the astrometric uncertainties by at most only 30% and on average by only 10%.

3.3.2. *Orbital Fit Results*

Estimates of the central dark mass’ properties from the simultaneous fit are reported in Table 2 . The central dark mass is estimated to be $(4.0 \pm 0.3) \times 10^6 (\frac{R_o}{8kpc})^3 M_\odot$. While this is consistent with that inferred from the orbit of S0-2 alone (Ghez et al. 2003, Schödel et al. 2002), its uncertainty is a factor of 2 - 5 times smaller due to the additional information offered by S0-16 and S0-19. This makes distance, which is fixed in all the orbital analyses reported thus far, the limiting uncertainty for the first time; the 0.5 kpc uncertainty in the Galactic center distance (Reid 1993) contributes an additional 19% uncertainty in the estimated mass, beyond that reported in Table 2. Similarly to the mass, the inferred center of attraction agrees well with the results from the analysis of S0-2’s orbit by Ghez et al. (2003). In contrast to the mass, the location is not significantly improved in the simultaneous fit (± 1.4 mas), because stars beside S0-2 add little information to it. The estimate on the dark mass’s motion on the plane of the sky is the first such estimate derived from orbital fits. While a single star’s orbital trajectory can, in principle, constrain this motion, in this solution it is primarily constrained by the closest approaches of S0-2, S0-16, and S0-19 and their span of periape passage times of 5 years. The inferred motion of the dark mass on the plane of the sky is 32 ± 25 km s⁻¹, consistent with no motion. Overall, simultaneously fitting the stellar orbital motion has allowed significant improvements in the derivation of the central dark object’s properties.

With the central parameters constrained simultaneously by multiple stars, the precision with which each star’s orbital elements can be determined is also greatly improved compared to that obtained from an independent orbit analysis. Table 3 lists the parameters specific to the individual stars from the simultaneous fit. Over the course of this study (1995 - 2003), these stars have either undergone periape passage or are remarkably close to periape. Consequently their periape distances are well defined and have values as small as 90 AU, in the case of S0-16, and as large as 3100 AU, in the case of S0-5. Similarly, the orbits’ orientations are remarkably well determined for stars that in some cases have undergone only a small fraction of their orbit. In these cases, this is possible because other stars are defining the central mass’ properties.

There are clear selection effects in this study that must be understood and accounted for before the ensemble properties of the sample can be studied. Since a star has to experience acceleration in the plane of the sky of greater than 2 mas y⁻² to be included in the orbital analysis, there is an observational bias towards detecting stars in eccentric orbits at periape, in spite of the fact that a star spends most of its time away from periape. Stars experience their largest acceleration near periape, at a projected distance which scales as $q = A(1 - e)$. For a given semi-major axis above ~ 3200 AU, this allows stars in highly-eccentric orbits

to have detectable accelerations near their closest approach, while stars on low-eccentricity orbits will be below the detection threshold in all parts of its orbit. Figure 3 quantifies these effects based on the fraction of time a face-on orbit experiences accelerations larger than our threshold value. Three stars – S0-2, S0-16, and S0-20 – lie in the parameter space that is unbiased, 2 stars – S0-1 and S0-19 – reside in a region that is mildly biased (<50% effect), and the last 3 stars – S0-3, S0-4, and S0-5 – are detected only because they are on eccentric orbits and remarkably close to periaapse passage compared to their orbital periods. The excess of high eccentricity orbits in our sample is therefore a consequence of an observational bias; restricting the analysis to the 5 stars for which the bias is <50% effect, we find 3 stars with eccentricities greater than 0.87, which is statistically consistent with isotropy, if we assume that an isotropic system has a cumulative probability distribution $\propto e^2$. The distribution of semi-major axes is also noteworthy. While there are no observational selection effects against it, there is a distinct lack of stars as bright as those tracked in this study ($K \lesssim 15.5$) having semi-major axes $\lesssim 1000$ AU, and likewise apoapse distances of $\lesssim 1800$ AU. The other end of these distributions, however, are not seen due to selection effects.

In contrast to the shape of the orbit, its orientation should be unaffected by observational bias. To fully describe the orientations of the orbits, it is necessary to specify the directions of two vectors, one normal to the orbital plane, such as the angular momentum vector, and one along the semi-major axis, such as the direction to apoapse. For S0-2, which has both astrometric and radial velocity measurements, the full three-dimensional orbit is unambiguously determined. For the stars with only astrometric measurements available, however, a degeneracy exists from a possible reflection about the plane of the sky; we therefore assume that these orbits are oriented such that the unit angular momentum and apoapse direction vectors are in the same hemisphere as those quantities derived for S0-2. Figures 4 and 5 show the directions for these unit vectors. While the directions of the angular momentum vectors do not appear cluster, indicating that there is no common orbital plane, the vectors in the direction of apoapse appear to be non-random. To quantify the significance of this result, we fit a plane through these data points, both assuming that the apoapses lie in one hemisphere⁷ or that some lie on the opposite side, making the $2^{8-1} = 128$ different combinations of $\pm z$ orientations of all orbits except S0-2, whose line of sight orientation is not degenerate. A Monte Carlo simulation of random drawings of 8 stars then reveals that the same χ_{dof}^2 or better occurs for a random distribution in only 6.6% of the time assuming that they all lie in one hemisphere and 3.5% of the time for the best of the 128 combinations. This suggests that at the 2σ level the distribution of apoapse directions is non-random.

⁷The 2-fold degeneracy in the inclination angle moves the points to the other hemisphere, so there is no way to differently populate the hemisphere shown with this sample of stars.

4. Discussion

4.1. The Case for and Properties of the Central Supermassive Black Hole

Stellar orbits provide the most direct measure of the amount of dark matter concentrated at the center of the Galaxy. Compared to masses inferred from the velocity dispersion measurements, the mass derived from multiple orbits, $(4.0 \pm 0.3) \times 10^6 M_\odot$, is a factor of 2 higher than that estimated by a non-parametric approach presented by Chakrabarty & Saha (2001), which is supposed to be the most robust approach, and is somewhat less discrepant with the parametric approaches (e.g., Ghez et al. 1998; Genzel et al. 2000). Since the mass estimates from the velocity dispersion measurements and orbital fits have all assumed the same distance and depend on distance as R_o^3 , the assumptions about distance are not the source of this mass discrepancy. By simultaneously fitting multiple orbits, we now have only one additional free parameter in the Keplerian orbit model, that of the black hole’s motion along the line of sight. Given the small values for its motion on the plane of the sky, this last parameter is unlikely to have any significant effect on the estimated mass. The two possibilities therefore lie in problems with the mass estimates from the velocity dispersions. First, the mass estimates could be biased by the weighting schemes used to calculate the velocity dispersions. While roughly 100 stars have reported proper motion values (Ghez et al. 1998; Genzel et al. 2000), only 18 of these have $S/N > 5$ and half of them have $S/N < 3$, making the velocity dispersion bias term non-negligible and skewing the distributions towards the few high velocity stars. Second, the projected mass estimators could be biased by the properties of the central stellar cluster. Specifically, both the level of anisotropy and the slope of the stellar density distribution can significantly alter the values inferred from standard projected mass estimators (Genzel et al. 2000). Different results have been reported both for the presence of anisotropy (Ghez et al. 1998; Genzel et al. 2000; Genzel et al. 2003) and the radial distribution of stars (Scoville et al. 2003; Genzel et al. 2003). While a full exploration of these effects is outside the scope of this paper, here we emphasize that the orbital mass is more robust and should be used in all future characterizations of the Galaxy’s central dark mass concentration.

Stellar orbits confine the central dark mass of $(4.0 \pm 0.3) \times 10^6 (\frac{R_o}{8kpc})^3 M_\odot$ to within 90 AU, the closest approach of S0-16, implying a minimum density of $4 \times 10^{16} M_\odot / pc^3$ for the central dark mass. This is a factor of three larger than that inferred from S0-2 (Schödel et al. 2002; Ghez et al. 2003) and four orders of magnitude larger than estimates from measurements of acceleration vectors (Ghez et al. 2000; Eckart et al. 2002). At this density, the two existing alternative explanations to a supermassive black hole for the compact dark object found at the center of the Galaxy become significantly less tenable. Any cluster of dark objects, such as those considered by Maoz (1998), would have a lifetime of a mere $\sim 10^5$ years, owing to

gravitational instability, which is significantly shorter than the age of the Galaxy, making this a highly unlikely explanation for the central dark mass concentration. For the fermion ball hypothesis (Viollier et al. 1993), the mass of the constituent particles is now required to be $73keVc^{-2}(\frac{0.3}{R})^{3/8}(\frac{2}{g})^{1/4}(\frac{4.0 \times 10^6}{M})^{1/8}$, where R and M are the radius in milli-pc and mass in M_{\odot} of the fermion ball, respectively, and g is the spin degeneracy factor of the fermion; this is 5 orders of magnitude larger than the current limits on degenerate neutrino species (Spergel et al. 2003), rendering the fermion ball hypothesis also highly unlikely. With the Galaxy’s central dark mass now confined to a radius equivalent to $1000 \times$ the Schwarzschild radius of a $4 \times 10^6 M_{\odot}$ black hole, the multiple stellar orbits present the strongest case yet for a supermassive black hole at the center of the Milky Way galaxy.

The measured linear motion of the central black hole on the plane of the sky limits the mass of any possible companion black hole. With a 1σ upper limit of 30 km/s, the mass of any possible companion black hole is constrained to be less than $\sim 2 \times 10^5 (R/16,000 AU)^{1/2} M_{\odot}$, where R is the distance of the companion black hole from the central black hole; the generalization of this limit to other radii works as long as the black hole companion lies outside the orbits that contribute to the determination of the central dark object’s properties (Table 3) and that the orbital period is long compared to the duration of the study, 8 years. A related measurement comes from upper limits inferred for the motion of the radio source Sgr A*, which is assumed to be associated with the central black hole (see discussion in §4.2). Backer & Sramek (1999) and Reid et al. (1999) published upper limits of ~ 20 km s^{-1} , which are comparable to our limits, and, more recently, Reid et al. (2003b) announced a more constraining upper limit of 8 km s^{-1} . However, the infrared and radio measurements are fundamentally different. In the infrared, the black hole’s motion is measured with respect to the central stellar cluster, which traces the local barycenter, while in the radio, Sgr A*’s motion is derived with respect to background quasars, so motions of the black hole along with the central stellar cluster as well as the solar parallax show up in this measurement. Therefore, while the radio upper limit on the motion of Sgr A* is smaller than the infrared upper limit on the motion of the black hole, the later is a more direct measure of the upper limit for the reflex motion from a black hole companion.

In the context of other galaxies, the Milky Way’s central dark mass concentration distinguishes itself in terms of both its inferred density and mass. The Galaxy’s central minimum dark mass density now exceeds the minimum dark matter density inferred for NGC 4258 (Greenhill et al. 1995; Miyoshi et al. 1995) by five orders of magnitude, reinforcing the Milky Way as the strongest case for a black hole at the center of any normal type galaxy. This also allows the fermion ball hypothesis as a universal alternative explanation for supermassive compact objects to be ruled out. For objects composed of the minimum mass particles imposed by the stellar orbits in the Galactic center, the maximum mass is

$1 \times 10^8 M_\odot \left(\frac{73 \text{keV}}{mc^2}\right)^2 \left(\frac{2}{g}\right)^{1/2}$, from the Oppenheimer-Volkoff limit (Munyaneza & Viollier 2002). This is less massive than half of the supermassive compact objects that have been identified thus far (cf., for example, compilation in Tremaine et al. 2002), thereby eliminating an all-encompassing Fermion ball hypothesis.

In contrast to its high minimum central dark mass density, the Milky Way appears to harbor the least massive supermassive black hole. It therefore potentially has an important role to play in assessing the M_{bh} vs. σ relations (e.g., Ferrarese & Merritt 2000; Gebhardt et al. 2000). However, the current impact of the Milky Way on the M_{bh} vs. σ relation is limited by uncertainties in the determination of its bulge velocity dispersion (Tremaine et al. 2002). Nonetheless, the higher mass value from the orbits brings our Galaxy into better agreement with the M_{bh} vs. σ relationship derived from a large sample of galaxies (e.g., Tremaine et al. 2002, Merritt & Ferrarese 2001).

4.2. Sgr A* and other Possible Counterparts to the Central Black Hole

The orbits provide very precise information on the location and kinematics of the central supermassive black hole, allowing us to explore its association with the radio source Sgr A* and any possible near-infrared counterparts. Relative to the dynamically determined position of the central dark mass, which is known to within 1.5 mas (1σ), the inferred infrared position of Sgr A*, which is less accurately known, ± 7 mas (1σ ; see §3.2 and Reid et al. 2003), is offset by a mere 5.2 mas S and 12 mas E; the two positions therefore appear to be consistent to within 1.9σ . Furthermore, using the kinematics of S0-2 from Ghez et al. (2003) and the upper limit on the motion of Sgr A*, Reid et al (2003) argue that Sgr A* has a minimum mass of $4 \times 10^5 M_\odot$, consistent with the black hole mass estimated from orbital motion. Given the agreement in position, velocity (discussed in §4.1), and mass, it appears that Sgr A* is indeed associated with the black hole at the Galaxy’s center.

Identifying near-infrared counterparts to the central black hole is a difficult task, given the high stellar densities and velocities, the modest stellar intensity variations in this region, and the maximal confusion at that location. S0-19 serves as a good illustration of these challenges; its large proper motion and strong curvature in a crowded region makes it challenging to track and led Genzel et al. (1997) to propose their 1996.43 detection of this source (their label S12) as the best candidate for the infrared emission from the central black hole. It is now clear that S12 is simply one data point in the trajectory of the high velocity star S0-19 that, in 1996 ⁸, was coincident to within 1σ with the relatively crude position of Sgr

⁸S0-19 was detected by Ghez et al. (1998) in 1995 with two possible counterparts identified in 1996.

A* as reported by Menten et al. (1997), but it is recognized here to be 70 mas, or 16σ , off from the newly determined location of the black hole

The search for infrared counterparts to the central black hole is greatly facilitated by the use of stellar orbital motions to refine its location by more than an order of magnitude. In 1995 and 2000 - 2002, a bright star was located within 50 mas of this location, preventing a faint counterpart from being easily detected. In the remaining years, 1996-1999 and 2003, there is no source detected by the relatively conservative source identification criteria set forth in §3.1 within 3σ of the dynamically determined location of the black hole. We therefore infer that no source as bright or brighter than ~ 15.5 , the magnitude of the faintest stars we were reliably able to track⁹ in this region in all of the maps, was coincident with our inferred black hole position.

4.3. The Origin of the Central Stellar Cluster

The orbital parameters derived here provide important clues for understanding the origin of the Sgr A* cluster stars, which appear to have hot photospheres similar to those of massive young stars (Genzel et al. 1997; Eckart et al. 1999; Figer et al. 2000; Gezari et al. 2002; Ghez et al. 2003). In the context of the luminous He I emission line stars, which are located an order of magnitude further from the black hole than the Sgr A* cluster stars, several ideas have been proposed to account for apparently young stars in a region whose current conditions seem to be inhospitable to star formation: 1) that the early-type stars are the result of stellar mergers in this dense environment, 2) that they are exotic objects masquerading as normal stars, 3) that they were formed by a cataclysmic compression of an already dense cloud which wandered into this region as a result of sudden accretion onto the GBH, and 4) that they were formed elsewhere as part of a massive cluster, but migrated inwards rapidly by dynamical friction. Here, we briefly examine each of these hypotheses in turn in the context of the Sgr A* cluster stars.

Stellar mergers of relatively old stars can, if the stellar density is sufficiently large, produce stars massive enough to appear as main-sequence OB stars. There are four challenges to this hypothesis for the stars in the Sgr A* cluster. First, several successive mergers of stars of increasing mass are required to produce a star resembling S0-2 ($\sim O9.5$, $M \sim 15M_{\odot}$),

With limited time coverage, Ghez et al. (1998) were not able to definitively identify either as the correct counterpart to either S0-19's 1995 position or Sgr A* and therefore it was not included in their proper motion sample.

⁹Many sources fainter than 15.5 are identified in this region.

unless the mass segregation in this region has been so strong that only stars having $\gg 1M_{\odot}$ are left. Second, as the merger products become more massive, their nuclear lifetimes decrease, so that there is less time available for the next merger event in the sequence. Using a Fokker-Planck approach, Lee (1996) investigated the stellar merger hypothesis for the massive emission-line stars in the central parsec, and concluded that an insufficient number of them is likely to be present. The Sgr A* cluster stars, however, are much more concentrated toward the center where the stellar density is maximized (Genzel et al. 2003) and the collision time is correspondingly shorter, so in this respect, merger events may be relatively favored there. However, the third challenge is that the velocity dispersion of stars near the Galactic black hole, 400 km s^{-1} at 0.01 pc (Ghez et al. 1998) is comparable to the escape velocity from the surface of a main-sequence O9.5 star, $\sim 1000 \text{ km s}^{-1}$, so collisions in the volume occupied by the Sgr A* cluster stars are therefore less likely to lead to mergers and mergers that do occur are likely to be accompanied by significant mass loss (Freitag & Benz 2002). In terms of the kinematic signatures, this mechanism most likely produces randomly oriented orbits, which is inconsistent with the possible bias observed in the apoapse directions shown in Figure 5. A fourth consideration which may disfavor the collisional mechanism is the relatively normal rotation rate of S0-2 (Ghez et al. 2003). Alexander & Kumar (2001 ApJ) have found that tidal encounters between main-sequence stars in the central cluster can eventually spin up those stars to near break-up speed. Colliding stars effectively represent an extreme example of this phenomenon, so merger products should be much more rapidly rotating than S0-2 appears to be. Of course, the apparent rotation rate of S0-2 can be attributed to a particular, low-probability orientation, so the measurement of absorption-line widths in just one additional member of the cluster should clarify this point. A further stochastic indicator of merger history is the distribution of orbital eccentricities of the SgrA* cluster stars. A succession of mergers is likely to favor low-eccentricity orbits, so it is not yet clear whether the biased distribution of relatively eccentric orbits can be consistent with the merger scenario. Further calculations are clearly required to assess the importance of this complex mechanism.

Another suggestion to account for the Sgr A* cluster stars without invoking star formation is that they may be exotic objects. This catch-all category includes a number of possibilities. For example, it is reasonable to expect that stellar remnants such as neutron stars and black holes sink into the central few milli-parsec as a result of dynamical mass segregation (Morris 1993; Lee 1996; Miralda-Escudé & Gould 2000). Mergers of these remnants with normal stars could produce Thorne-Zytkow objects, or, in the case of black hole remnants, something with dubious long-term stability. However, Thorne-Zytkow objects are expected to appear as red giants or supergiants rather than massive blue stars, and may be unstable; likewise, stable stellar objects with black hole cores have yet to be described.

If the stellar remnant that undergoes a merger is a white dwarf, then a “reborn star” results, and it could be suitably luminous. However, such an object would probably be a red giant rather than an early-type star, and in any case, the white dwarf precursors is likely to have migrated out of the central region because of its low mass. Another, slightly less exotic possibility for the Sgr A* cluster stars is that they be the exposed, hot cores of tidally stripped red giant stars. Indeed, there appears to be a paucity of red giants in the inner 0.2 pc of the Galaxy (Sellgren et al. 1990; Genzel et al. 1996), suggesting that red giant atmospheres are collisionally removed there, possibly by collisions with binaries (Davies et al. 1998). However, the luminosity of the exposed stellar cores may be too small to account for the Sgr A* cluster stars (e.g., Schönberner 1981, 1983).

The third category of hypotheses is that the early-type stars really did form recently *in situ*. To do this, the parent cloud would have to have undergone violent compression to densities exceeding the limiting Roche density.¹⁰ This hypothesis warrants consideration because the mechanism for violent compression of any cloud passing close to the black hole is innate to the model. A dense cloud brought within 0.02 parsecs of the Galactic black hole would unavoidably lead to a high rate of accretion onto the black hole. If the onset of this accretion is rapid, the resultant release of accretion energy would be powerful enough to compress the cloud. Morris, Ghez & Becklin (1999) proposed that this process can manifest itself as part of a limit cycle involving the circumnuclear disk (CND). This disk currently has a central cavity of 1 parsec radius, presumably because of the outgoing ram pressure of the winds from the cluster of luminous, early-type stars in the central parsec. However, as the lifetimes of these stars is $\sim 10^7$ years, and because the CND itself undergoes viscous evolution on times more comparable to the orbital time at the inner radius, $\sim 5 \times 10^4$ years, the inner edge of the CND will migrate toward the central black hole on a time scale comparable to the stellar evolution time. When the first portions of the CND reach the central black hole, the outgoing shock resulting from the accretion event provokes massive star formation in the now nearby disk by strong compression. The strong winds from these stars cause the inner disk boundary to recede and the cycle begins anew. A weakness of this hypothesis is the magnitude of the required compression. While the density of a cloud which has migrated close to the black hole might be substantially larger than the densities so far inferred for any of the gas in the region, it is difficult to see how even the most effective compressive

¹⁰Tidal compression may be a contributor: a cloud moving toward the center on a purely radial trajectory will experience a compression in two-dimensions, although this would be counteracted by distention in the radial dimension, so that the net compression would not be a strong function of radius, and is not likely, by itself, to be able to raise the density by the many orders of magnitude necessary. In addition, any non-radial motion would imply a tidal shear in the azimuthal direction which would also counteract the tidal compression.

event can bring gas up to the limiting Roche density. Furthermore, this scenario is expected to form stars with a common or biased direction for the angular momentum vectors and random apoapse directions, which is contrary to the observations.

The fourth hypothesis which has been considered is that the early-type stars in the central parsec formed well outside the central parsec, but migrated inward under the action of dynamical friction on time scales substantially less than their nuclear time scale, $\sim 10^7$ years. This is not possible for individual stars (Morris 1993), but Gerhard (2001) has pointed out that, because the dynamical friction time scale is inversely proportional to an object's mass, sufficiently massive clusters can migrate to the central parsec from radii of tens of parsecs within the required time, especially if they remain bound to their parent cloud. This hypothesis has been investigated numerically by Kim & Morris (2003) and Portegies-Zwart & McMillan (2003), who clarify that very massive clusters are required – $10^{5-6} M_{\odot}$, far more massive than even the extreme (for our Galaxy) Arches and Quintuplet clusters (e.g., Figer, McLean, & Morris 1999, Figer et al. 2002), Core collapse is inevitable in the massive, dense clusters required for the cluster inspiral hypothesis. This process helps ensure that, in spite of tidal stripping of stars outside the cluster core as the cluster migrates inward, there remains a tightly bound, cluster core that survives intact into the central parsec. However, Portegies-Zwart and McMillan (2002, see also Rasio, Freitag, & Gürkan 2003) have raised the possibility that such core collapse in sufficiently massive clusters proceeds all the way to the formation of an intermediate-mass black hole (IBH), which can carry cluster stars in with it as it spirals inward by dynamical friction. The implications of such a cluster-produced IBH for the distribution of early-type stars in the central parsec have recently been investigated by Hansen & Milosavljevic (2003). They argue that the HeI emission-line stars in the central parsec have been tidally stripped from the IBH during successive passages near the supermassive black hole, but that they retain a memory of the IBH orbit. Furthermore, cluster evaporation during the inspiralling process leads to a marked decrease in the effectiveness of this process; a remnant core of an initially globular-cluster-mass cluster can reach the central parsec only by distributing a large number of early-type stars at all radii, whereas there is currently no evidence for a young population beyond the central parsec. In addition, Kim & Morris (2003) find that the mass of stars reaching the central parsec, for any feasible initial cluster mass, substantially exceeds the mass of early-type stars in the central parsec cluster. Further investigations of this hypothesis are warranted, though it currently appears to suffer from a number of difficulties.

Both the *in situ* formation mechanism and the evaporating, inspiralling cluster mechanism will lead primarily to a disk of stars, the first because the inwardly migrating reservoir of gas inevitably forms a disk by virtue of its angular momentum, and the second because the stars lost from the cluster will retain a memory of the direction of the cluster angular

momentum. While most of the early-type emission-line stars in the central parsec appear to orbit in or near a well-defined plane (Levin & Beloborodov 2003), the stars in the SgrA* cluster do not. Levin & Beloborodov argue that the SgrA* cluster stars and the more distant emission-line stars all formed at about the same time in a starburst taking place in a thick accretion disk around SgrA*, but that the orbits of the SgrA* cluster stars have been altered by Lens-Thirring precession caused by the massive central black hole, so that their orbital angular momenta have been widely spread out. One alternative hypothesis for the tight orbits of the SgrA* cluster stars is that they have resulted from the tidal disruption of massive star binaries as stars presumably related to the HeI emission-line stars undergo relatively close passages by the supermassive black hole (Gould & Quillen 2003). These authors estimate that a sufficient number of single stars resembling S0-2 can be scattered onto orbits similar to those of the SgrA* cluster stars to explain that cluster, if they originate in binary systems undergoing close passage by the black hole. Multiple encounters with other stars in this region are required to bring the apoapse distances down to the range of values exhibited by the SgrA* cluster stars, i.e., far smaller than the typical orbital radii of the more massive emission-line stars. It remains to be seen whether this hypothesis can account for the possible non-random distribution of apoapse directions of the SgrA* cluster stars.

In the Hansen & Milosavljevic (2003) picture invoking an IBH, the SgrA* cluster stars are considered to have originally been among the population of stars which were tidally stripped from the cluster core/IBH, but they require a subsequent perturbation to have scattered them onto their present orbits. This perturbation can be due to one or more grazing collisions with other stars or to a new encounter with the IBH itself. The apoapse distances of these stars are largely constrained to lie within the periapse distance of the IBH, however, or they would eventually be scattered out of the region altogether. This hypothesis may be able to accommodate the non-random distribution of apoapse directions of the SgrA* cluster stars, if the primary perturber is the IBH and if it is on a somewhat eccentric orbit, because the last scattering these stars will have experienced is likely to then have taken place near the radius and direction of the IBH periapse.

In sum, there are serious difficulties or open questions associated with all of these hypotheses, although none of them can be definitively ruled out. The apparently non-random distribution of the apoapse directions, while based on only 8 stars, does favor the infalling cluster scenario for the production of the Sgr A* cluster stars, although better statistics and a resolution of the 2-fold degeneracy in those directions would improve the assessment. Additional orbits for stars in the vicinity of the central black hole should ultimately provide a sufficiently strong constraint to cull this list of possibilities. In the meantime, we are left with an interesting conundrum.

5. Conclusions

After almost a decade of diffraction-limited imaging at the Keck Telescopes, we have obtained the orbital solution for multiple stars. This orbital analysis has the advantage of simultaneously solving for a common set of properties for the central dark object, which not only reduces the uncertainties in the black hole’s mass and location compared to an analysis that treats each star independently, but also provides the first direct measure of the black hole’s velocity with respect to the central stellar cluster. Together, the stellar motions reveal a central dark mass of $4.0(\pm 0.3) \times 10^6 \left(\frac{R_o}{8kpc}\right)^3 M_\odot$ and confine it to within a radius of a mere 90 AU or equivalently $1,000 R_{sh}$, dramatically strengthening the case for a supermassive black hole, the location of which is now determined to within ± 1.5 mas. Consequently, the dark mass at the center of the Milky Way has become the most ironclad case of a supermassive black hole at the center of any normal type galaxy.

The precision of the proper motion and radial velocity measurements opens up additional new realms for dynamical studies in the Galactic Center. First is the possibility of doing a full orbital model, which also solves for the distance to the central black hole as well as its motion along the line of sight (Salim & Gould 1999; Ghez et al. 2003). While solving for the motion along the line of sight will require more years of radial velocity data on preferably several stars, only one more year of both astrometric measurements and radial velocity measurements for S0-2 alone should provide the most direct and precise estimate of the distance to the Galactic Center. A second opportunity is the possibility of detecting deviations from a Keplerian orbit. These might arise from precession of the periaapse distance due to general relativistic effects (Jaroszynski 1998; Fragile & Matthews 2000)¹¹ or an extended mass distribution (Rubilar & Eckart 2001), in the form of either an entourage of stellar remnants surrounding the central supermassive black hole, a spike of dark matter particles (Gondolo & Silk 1999; Ullio et al. 2001) or a binary black hole.

The stars that have been the tracers of the gravitational potential are themselves quite interesting. Their spectral feature suggest that they are young (<10 Myr). Since these stars currently reside in a region that is inhospitable to star formation, they are either old stars whose appearance has been significantly altered or they are young stars formed by an mechanism that is able to circumvent the challenges presented by the central black hole. This study, for the first time, uses the kinematics of stars in the Sgr A* cluster to shed light on this paradox. Among the notable properties are an eccentricity distribution that shows no statistically significant departures from an isotropic distribution, an apoapse distribution for

¹¹This would require the discovery of a star with a significantly smaller periaapse passage than has been found so far.

stars brighter than 15.5 mag that is truncated at 1800 AU, a random distribution of angular momentum vector directions, and a distribution of apoapse directions that is co-planar at the 2σ level. While none of the proposed mechanisms is free from difficulties, a bias in the apoapse direction distribution would favor an origin in a dense infalling cluster from which young stars are tidally stripped at the cluster’s closest approach of ~ 2000 AU. Additional orbits will help to clarify the ensemble kinematics of this unusual group of stars, which reside in a particular complex region.

The authors thank Joel Aycock, Randy Campbell, Bob Goodrich, David LeMignant, Chuck Sorensen, and Peter Wizinowich at the Keck Observatory for their help in obtaining the new observations, Gary Chanan for making it possible to phase the Keck Telescope on NIRC, Mark Reid for advance information on IRS 9 and 12N, and Mike Jura, Brad Hansen, Raoul Viollier, and Shelley Wright for helpful conversations. Support for this work was provided by the National Science Foundation grant AST-9988397 and the National Science Foundation Science and Technology Center for Adaptive Optics, managed by the University of California at Santa Cruz under cooperative agreement No. AST-9876783. The W.M. Keck Observatory is operated as a scientific partnership among the California Institute of Technology, the University of California and the National Aeronautics and Space Administration. The Observatory was made possible by the generous financial support of the W.M. Keck Foundation. The authors also wish to recognize and acknowledge the very significant cultural role and reverence that the summit of Mauna Kea has always had within the indigenous Hawaiian community. We are most fortunate to have the opportunity to conduct observations from this mountain.

A. Source Naming

Newly identified sources are named here using the convention introduced by Ghez et al. (1998), which was designed to directly convey relevant information about the location of the source relative to the position of Sgr A*. Originally, the Sgr A* position given by Menten et al. (1997) was adopted and the surrounding field was divided into concentric arcsecond-wide annuli centered on this position. Stars lying within the central circle, which has a radius of 1 arcsecond, were given names S0-1, S0-2, S0-3, etc. Stars lying in the annulus between radii of 1 to 2 arcseconds were given the names S1-1, S1-2, and so on. The number immediately following "S" thus refers to the inner radius of the annulus in which the star lies. The number following the hyphen was ordered in the sense of increasing distance from Sgr A* within each annulus at the time of its naming. In this scheme, newly identified sources are named by incrementing the number following the hyphen within each annulus and ordered in the sense

of increasing distance from Sgr A*. Since the original list within 1 arcsecond ended at 15, the newly identified stars begin with 16. S0-16, S0-17, and S0-18 were labeled by us in a recent spectroscopic paper (Gezari et al. 2001) and S0-19 and S0-20 were first presented at the Rees Symposium “Making Light of Gravity,” held in Cambridge, England (July 2002). Due to the motions of stars, and refinements in the location of Sgr A*, the current distance rank does not necessarily match the one at the time of discovery.

B. Absolute Astrometry

Estimates of the camera’s pixel scale and orientation, as well the position of Sgr A*, require tying the relative measurements to an absolute reference frame. This was done by obtaining multiple telescope pointings that allow the construction of mosaics covering the positions of Sgr A* and two SiO masers, IRS 7 and IRS 10EE in 1998 May, 1998 Aug, 1999 May, 1999 July, 2000 May, 2000 July, 2001 May, 2001 July. In 1999 July, a somewhat larger region was covered to include the positions of two additional masers, IRS 9 and 12N, which is used here as a check of our absolute astrometry analysis. Relative infrared positions IRS 7 and IRS 10EE are obtained by the same method described in §3.2 but using the larger mosaic maps and positional uncertainties determined by requiring that linear fits to their proper motion velocities produces a χ^2_{dof} of 1. Together, the infrared positions and radio positions, from Reid et al. (2003), provide the pixel scale, 20.457 ± 0.027 mas pix⁻¹, position angle of North with respect to NIRC columns in 1999 July, 0.40 ± 0.13 , and the location of Sgr A*, which is located to within ± 7 mas and is given in Table 4 with respect to the closest three IRS 16 sources.

The infrared positional uncertainties obtained in this procedure are larger than can be explained by uncertainties in the infrared centroids of these bright stars or the alignment of the map to a common epoch. This, most likely, reflects a small residual distortion in the NIRC camera ¹². The effects of distortion are minimized in our measurements of the Sgr A* cluster stars by always positioning them at the center of the field of view and carrying out the observations over similar ranges of parallactic angle during every observing run ¹³. In contrast, the masers not only occupied different camera positions, but were measured at

¹²A known distortion in the NIRC optics is corrected for in the individual exposures before the SAA maps are made, however any distortion introduced by the reimager (Matthews et al. 1996) has not been accounted for and is the likely source of additional measurement error.

¹³The rotator was turned off during this experiment so the direction of North with respect to the camera, the parallactic angle, changes throughout the night.

different times during the night, resulting in non-constant relative position vectors on the camera between each maser and Sgr A* from run to run. This, unlike the measurements of the stars within the Sgr A* cluster, maximally sampled the effects of distortion, which amount to a ~ 0.5 pixel offset from the center of the field of view to the edge (a 0.4% effect). This distortion is what dominates our uncertainties in the inferred infrared position of Sgr A* to 7 mas, which is comparable to the 10 mas accuracy obtained by Reid et al. (2003). In contrast, the distortion is not a significant effect for the relative stellar position measurements of stars in Table 1, which have a maximum displacement of $\sim 0''.2$ over the course of this study and therefore experience at most a ~ 1 mas offset from distortion.

REFERENCES

- Backer, D. C., & Sramek, R. A. 1999, *ApJ*, 524, 805
- Chakrabarty, D., & Sarah, P. 2001, *AJ*, 122, 232
- Davies, M. B., Blackwell, R., Bailey, V. C., Sigurdsson, S. 1998, *MNRAS*, 301, 745
- Eckart, A., & Genzel, R. 1997, *MNRAS*, 284, 576
- Eckart, A., Genzel, R., Ott, T., & Schödel, R. 2002, *MNRAS*, 331, 917
- Eckart, A., Ott, T., & Genzel, R. 1999, *A&A*, 352, L22
- Ferrarese, L., & Merritt, D. 2000, *ApJ*, 539, L9
- Fragile, P. C., & Mathews, J. 2000, *ApJ*, 542, 328
- Freitag, M., & Benz, W. 2002, *A&A*, 394, 345
- Figer, D. F. et al. 2000, *ApJ*, 533, L49
- Figer, D. F., McLean, I. S., & Morris, M. 1999, *ApJ*, 514, 202
- Figer, D. F., et al. 2002, *ApJ*, 581, 258
- Figer, D. 1995, Ph.D. Thesis, University of California, Los Angeles
- Gebhardt, K. et al. 2000, *ApJ*, 539, L13.
- Genzel, R., Eckart, A., Ott, T., & Eisenhauer, F. 1997, *MNRAS*, 291, 219
- Genzel, R., Pichon, C., Eckart, A., Gerhard, O. E., Ott, T., 2000, *MNRAS*, 317, 348

- Genzel, R. et al. (2003) astro-ph/0305423
- Genzel, R., Thatte, M., Krabbe, Kroker, H., & Tacconi-Garman, L. E. 1996, ApJ, 472, 153
- Gerhard, O. 2001, ApJ, 546, L39
- Gezari, S., Ghez, A. M., Becklin, E. E., Larkin, J., McLean, I. S., Morris, M. 2002, ApJ, 576, 790
- Ghez, A. M., Duchêne, G., Matthews, K., Hornstein, S. D., Tanner, A., Larkin, J., Morris, M., Becklin, E. E., Salim, S., Kremenek, T., Thompson, D., Soifer, B.T., Neugebauer, G., McLean, I. 2003, ApJ, 586, L127
- Ghez, A. M., Klein, B. C., Morris, M., & Becklin, E. E. 1998, ApJ, 509, 678
- Ghez, A. M., Morris, M., Becklin, E. E., Tanner, A., & Kremenek, T. 2000, Nature, 407, 349
- Gondolo, P., & Silk, J. 1999, Phys. Rev. Lett., 83, 1719
- Gould, A., & Quillen, A. C. 2003, ApJ, submitted (astro-ph/0302437)
- Greenhill, L. J., Jiang, D. R., Moran, J. M., Reid, M. J., Lo, K. Y., Claussen, M. J. 1995, ApJ, 440, 619
- Haller, J. W., Rieke, M. J., Rieke, G. H., Tamblyn, P., Close, L., & Melia, F. 1996, ApJ, 456, 194
- Hansen, B. M. S., & Milosavljević, M. 2003, ApJ, submitted (astro-ph/0306074)
- Jackson, J. M., Geis, N., Genzel, R., Harris, A. I., Madden, S., Poglitsch, A., Stacey, G. J., Townes, C. H. 1993, ApJ, 402, 173
- Jaroszynski, M. 1998, Acta Astronomica, 48, 653.
- Kim, S. S., & Morris, M. 2003, ApJ, submitted
- Lacy, J. H., Townes, C. H., Geballe, T. R., & Hollenbach, D. J., 1980, ApJ, 241, 132
- Lee, H.M., 1996, IAU 169, 215
- Levin, Y., & Beloborodov 2003, ApJ, 590, L33
- Lo, K. Y., Backer, D. C., Ekers, R. D., Kellermann, K. I., Reid, M., & Moran, J. M. 1985, Nature, 315, 124

- Maoz, E. 1998, *ApJ*, 494, L181
- Matthews, K., Ghez, A. M., Weinberger, A. J., and Neugebauer, G. 1996, *PASP*, 108, 615
- Matthews, K. and Soifer, B. T. 1994, *Astronomy with Infrared Arrays: The Next Generation*, ed. I. McLean, Kluwer Academic Publications (Astrophysics and Space Science, v. 190, p. 239)
- McGinn, M. T., Sellgren, K., Becklin, E. E., & Hall, D. N. B., 1989, *ApJ*, 338, 82
- Menten, K. M., Reid, M. J., Eckart, A., & Genzel, R. 1997, *ApJ*, 475, L111
- Merritt, D., Ferrarese, L. 2001, *ApJ*, 547, 140
- Miralda-Escudé, J., & Gould, A. 2000, *ApJ*, 545, 847
- Morris, M., 1993, *ApJ*, 408, 496
- Morris, M., Ghez, A. M., Becklin, E. E. 1999, *Adv. Spa. Res.*, 23, 959
- Miyoshi, M., Moran, J. M., Hernstein, J., Greenhill, L., Nakai, N., Diamond, P., & Inoue, M. 1995, *Nature*, 373, 127
- Munyanza, F. & Viollier, R. D. 2002, *ApJ*, 564, 274.
- Portegies Zwart, S. F., & McMillian, S. L. W. 2002, *ApJ*, 576, 899
- Portegies Zwart, S. F., McMillian, S. L. W., erhard, O. 2003, *ApJ*, in press (astro-ph/0304022)
- Rasio, F. A., Freitage, M., Gürkan, M. A., 2003, to appear in "Carnegie Observatories Astrophysics Series, Vol. 1: Coevolution of Black Holes and Galaxies," ed. L. C. Ho (Cambridge: Cambridge Univ. Press) (astro-ph/0304038)
- Reid, M. J. 1993, *ARA&A*, 31, 345
- Ried, M. J., Menten, K. M., Genzel, R., Ott, T., Schödel, R., & Brunthaler, A. 2003, *Astron. Nachr.*, Vol. 324, No. S1, Special Supplement "The Central 300 Parsecs of the Milky Way", ed. A. Cotera et al.
- Reid, M. J., Menten, K. M., Genzel, R., Ott, T., Schödel, R., & Eckart, A. 2003, *ApJ*, 587, 208
- Reid, M. J., Readhead, A. C. S., Vermeulen, R. C., Treuhaft, R. N. 1999, *ApJ*, 524, 816

- Rubilar, G. F., & Eckart, A. 2001, *A&A*, 2001, 372, 95
- Salim, S., & Gould, A. 1999, *ApJ*, 523, 633
- Sanders, R. H. 1992, *Nature*, 359, 131
- Schönberner, D. 1981, *A&A*, 103, 119
- Schönberner, D. 1983, *ApJ*, 272, 708
- Scoville, N. Z., Stolovy, S. R., Rieke, M., Christopher, M. H., Yusef-Zadeh, F. 2003, *ApJ*, in press (astro-ph/0305350)
- Sellgren, K., McGinn, M. T., Becklin, E. E., & Hall, D. N. B. 1990, *ApJ*, 359, 112
- Schödel, R. et al. 2002, *Nature*, 419, 694
- Spergel, D. N. et al. 2003, *ApJ*, submitted
- Tremaine, S. et al. 2002, *ApJ*, 574, 740
- Tsiklauri, D., & Viollier, R. D. 1998, *ApJ*, 500, 591
- Ullio, P., Zhao, H., Kamionkowski, M. 2001, *Phys. Rev. D*, 64, 1302
- Viollier, R. 2003, *Astron. Nachr.*, Vol. 324, No. S1, Special Supplement "The central 300 parsecs of the Milky Way", Eds. A. Cotera, H. Falcke, T. R. Geballe, S. Markoff

Table 1. Summary of Sources Identified within $0''.4$ of Sgr A*

Star Name	Other Name	$\langle K \rangle$ (mag)	R_{min}^a (arcsec)
S0-1	S1	14.7	$0''.136$
S0-2	S2	13.9	$0''.011$
S0-3	S4	14.2	$0''.175$
S0-4	S8	14.5	$0''.284$
S0-5	S9	15.1	$0''.319$
S0-16	...	15.3	$0''.003$
S0-19	...	15.6	$0''.033$
S0-20	...	15.5	$0''.154$
S0-6	S10	14.1	$0''.375$
S0-8	...	15.9	$0''.395$
S0-17	...	15.8	$0''.129$
S0-21	...	15.1	$0''.012$
S0-22	...	15.8	$0''.100$
S0-23	...	16.2	$0''.104$
S0-24	...	15.3	$0''.144$
S0-25	...	16.6	$0''.175$
S0-26	...	16.9	$0''.193$
S0-27	...	16.6	$0''.269$
S0-28	...	17.7	$0''.317$
S0-29	...	16.3	$0''.319$
S0-30	...	16.4	$0''.354$
S0-31	...	15.1	$0''.380$

Note. — Sources above the line have significant accelerations, revealing orbital solutions.

^aMinimum projected separation during the 1995-2003 time interval.

Table 2. Central Dark Mass Properties from Simultaneous Orbital Fit to Multiple Stars

Parameter	Estimated Value
Mass ($10^6(\frac{R_o}{8kpc})^3 M_\odot$)	3.99 ± 0.34
Position with Respect to S0-2 in 2003.0 (mas):	
Δr_{RA}	-34.67 ± 1.55
Δr_{DEC}	-54.13 ± 1.25
Proper Motion Relative to Central Cluster (mas y^{-1}):	
V_{RA}	-0.81 ± 0.67
V_{DEC}	-0.23 ± 0.74

Table 3. Stellar Orbital Parameters from Simultaneous Orbital Fit

Star	P (yrs)	A^a (mas)	T_o (yrs)	e	i (deg)	Ω^b (deg)	ω (deg)	q^a (AU)	Q^a (AU)
S0-2	15.02 (0.68/0.76)	120.7 (4.5)	2002.335 (0.013)	0.8763 (0.0063)	133.6 (1.7)	45.4 (1.7)	247.1 (2.3)	119.5 (3.9)	1812 (73)
S0-16	29.9 (6.8/13)	191 (24)	2000.243 (0.037)	0.943 (0.019)	101.1 (1.7)	49.1 (1.2)	166.1 (2.8)	87 (17)	2970 (560)
S0-19	71 (35/11000)	340 (220)	1995.639 (0.083)	0.889 (0.065)	35.9 (4.5)	57 (33)	134 (21)	301 (41)	5100 (3600)
S0-20	43.5 (8.6/19.3) ^c	256 (36/72)	2005.1 (1.1)	0.40 (0.11)	25 (13)	60 (45)	267 (34)	1230 (230)	2900 (1000)
S0-1	86 (18/31)	387 (63)	1997.1 (8.6)	0.32 (0.11)	121.0 (2.2)	153 (14)	257 (82)	2100 (240)	4090 (950)
S0-3	105000 (47000)	390000 (150000/770000)	2005.9 (1.1)	0.9972 (0.0012)	84.8 (1.0)	66.8 (1.0)	3.6 (4.3)	2340 (48)	1680000 (750000) ⁻
S0-4	13000 (12000/ ∞)	11000 (95000)	1989.32 (0.37)	0.9965 (0.0016)	74.8 (7.9)	109.8 (8.5)	253 (14)	300 (260)	170000(10 ⁶) ^c
S0-5	7700 (7200/ ∞)	7700 (7200/ ∞)	2001.1 (3.3)	0.95 (0.7/0.05) ^c	86.8 (1.1)	152.6 (0.7)	350.0 (9.6)	3100 (92)	120000 (115000/ ∞)

Note. — The first 3 stars represent a single joint solution. Each star below the line represents a four-star solution with the first 3 stars (see §3.3.1). Values in parentheses are 1σ uncertainties from the covariance matrix that takes into account the measurement uncertainties. When two values are given, the uncertainties are asymmetric, with the first number giving the low 1σ value and the other the high 1σ value.

^aThe semi-major axis (A), periaapse distance (q), and apoapse distance (Q) are not independent variables, but are reported here for convenience and to provide a proper accounting of their uncertainties.

^bLongitude of the node is given for the node lying in the East quadrants, except for S0-2 where it is the ascending node.

^cFixed parameter in the fit. The error corresponds to an allowable range.

Table 4. Absolute Astrometry of IRS 16 Sources Relative to Sgr A* in 1999.99

Source	ΔRA (arcsec)	ΔDEC (arcsec)	v_{RA} (mas y ⁻¹)	v_{DEC} (mas y ⁻¹)
IRS 16C	1.118 ± 0.007	0.51 ± 0.01	-9.5 ± 0.7	7.9 ± 0.9
IRS 16NW	-0.10 ± 0.006	1.22 ± 0.01	5.1 ± 0.8	2.4 ± 1.9
IRS 16NE	2.832 ± 0.008	1.13 ± 0.01	2.8 ± 0.9	-8.7 ± 2.0

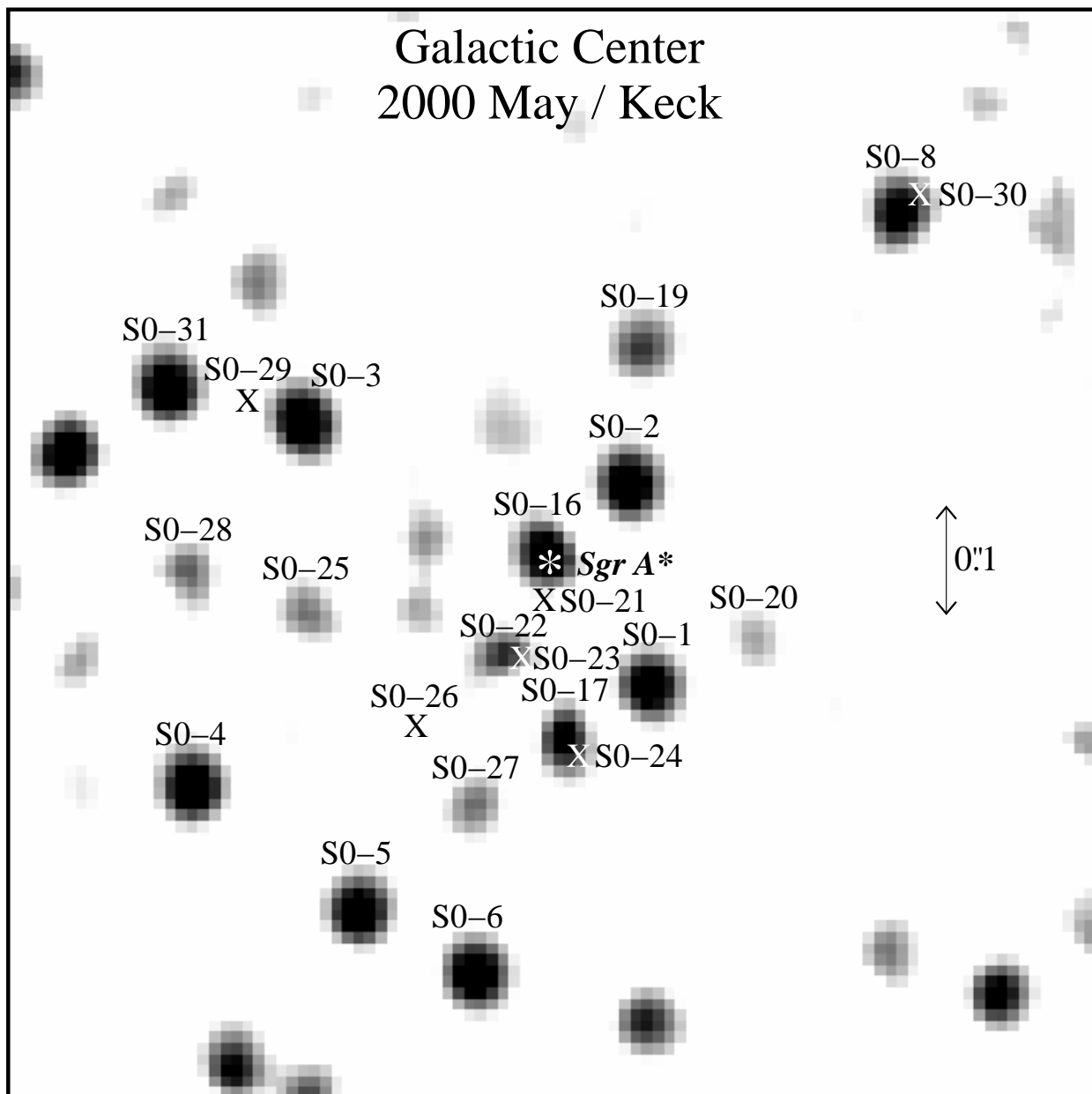


Fig. 1.— The central $1'' \times 1''$ of the cross-correlation (or match filter) map for the 2000 May data set. Of the 22 sources identified in this study by the criteria described in §3.1, 16 are seen in this map. The remaining six, marked with crosses, are missed in this particular map either due to confusion or source variability. An asterisk denotes Sgr A*'s position in the infrared reference frame. The criteria used for source identification are still quite conservative as there are three unlabeled peaks that are most likely real sources, within $0.4''$ of Sgr A*.

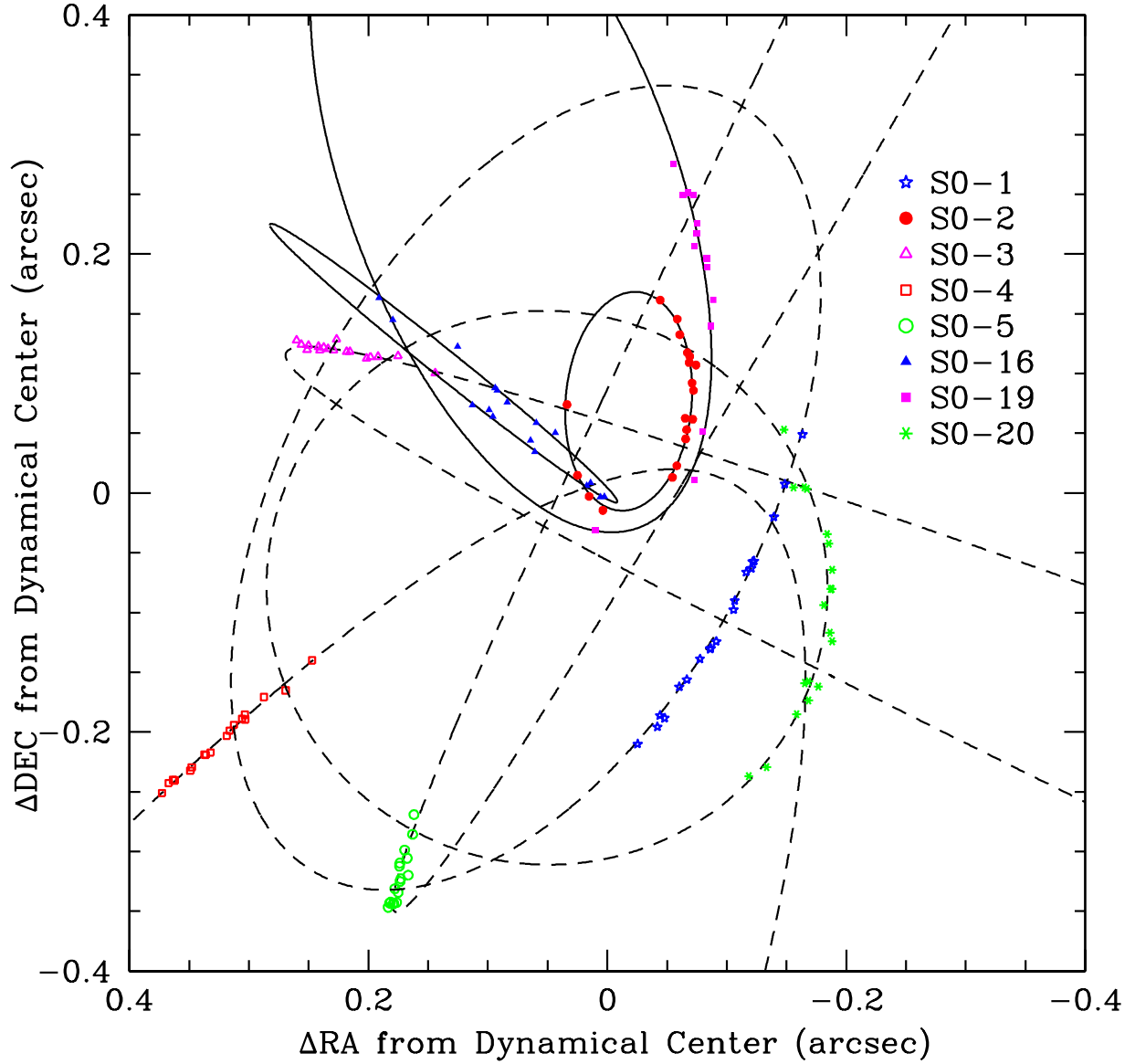


Fig. 2.— Astrometric positions and orbital fits for 8 stars, within the central $0''.8 \times 0''.8$ of the Galaxy, that show significant deviation from linear motion. The proper motion measurements were obtained at the Keck telescopes between 1995 and 2003, have uncertainties that are comparable to the size of the points, and are plotted in the reference frame in which the central dark mass is at rest. Overlaid are the best fitting simultaneous orbital solutions, which assume that all the stars are orbiting the same central point mass. The orbital solutions for the three stars that constrain the properties of the central dark object are delineated by solid lines and the joint orbital solutions for the remaining stars are shown with dashed lines.

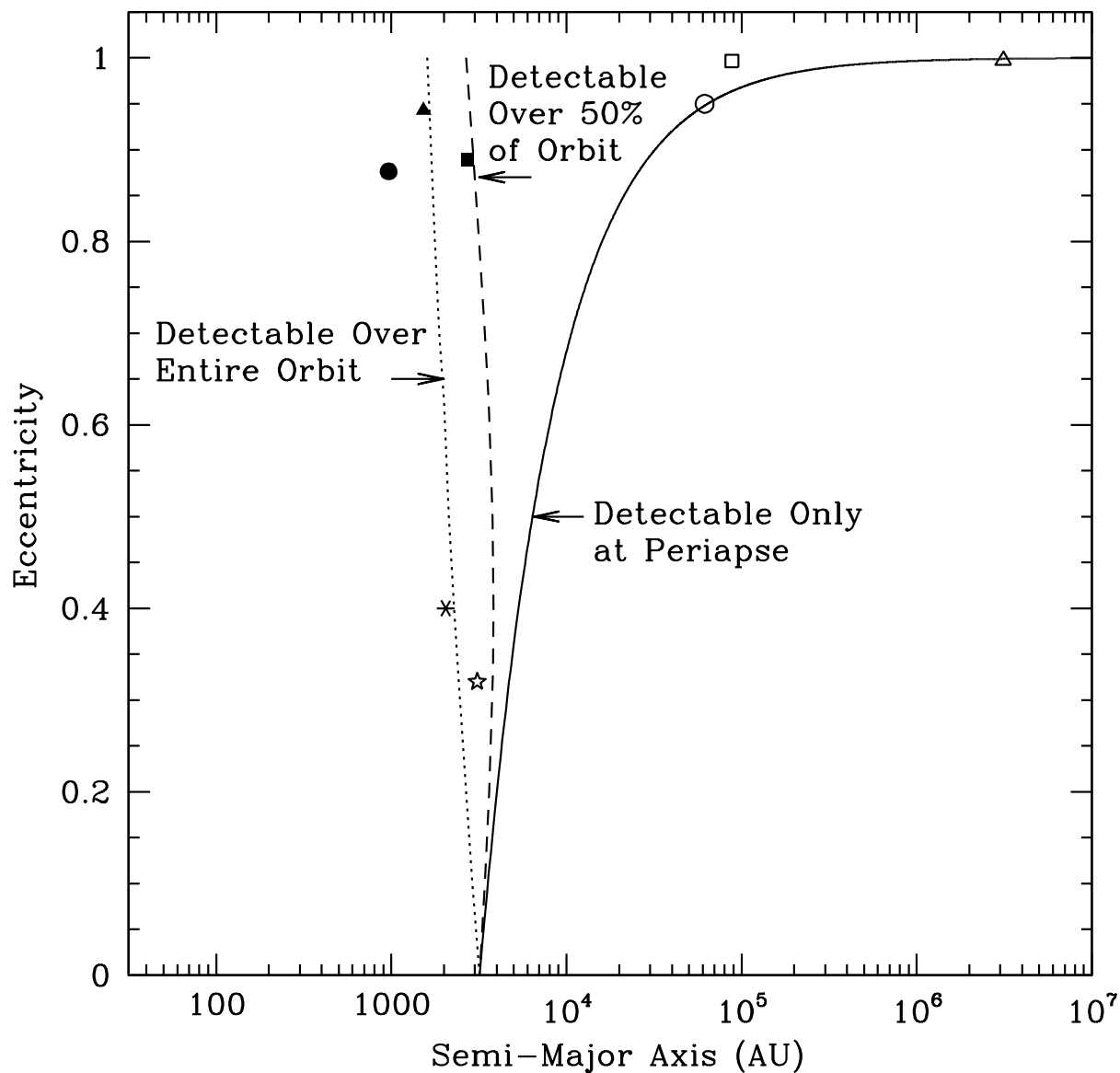


Fig. 3.— Eccentricity vs. Semi-Major Axis. Orbital parameters for the 8 stars included in this study are plotted using the same symbol key presented in Figure 2. The observational selection effects are quantified by the fraction of time a face-on orbit experiences acceleration larger than our threshold value of $2 \text{ mas } y^{-2}$, with the cases of 100% of the orbit (dotted), 50% of the orbit (dashed), and only periastron passage (solid) shown.

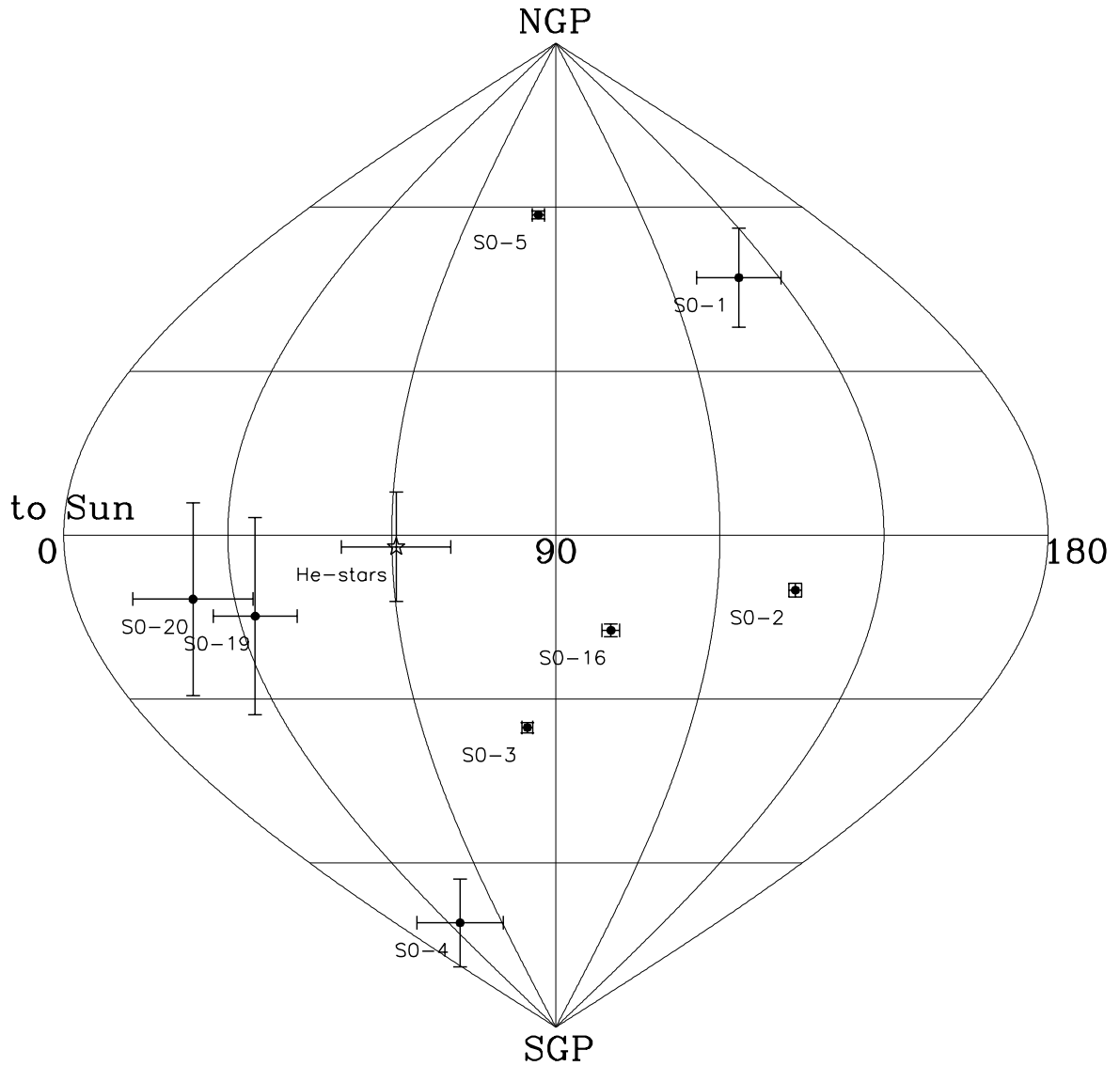


Fig. 4.— Positions of the angular momentum vectors for an observer at the center of the Galaxy. Only one hemisphere is shown (east as seen from the Earth), since the degeneracy of the inclination sign makes it impossible to know which hemisphere a vector points, except for S0-2. If the orbits were to be co-planar the angular momentum vectors would cluster, which we do not see. The normal to the plane of the He I stars found by Levin & Beloborodov (2003) is also indicated.

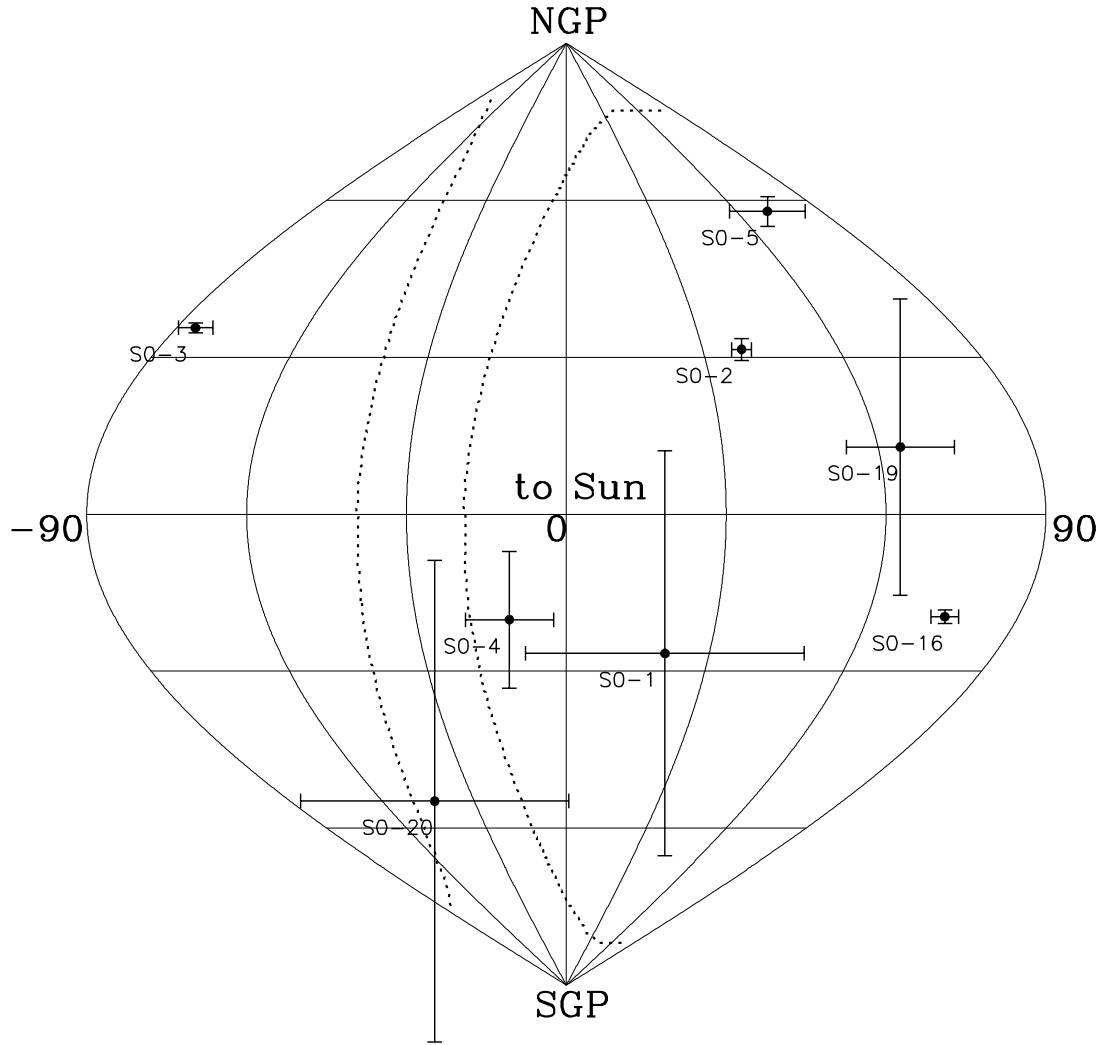


Fig. 5.— The locations of apocenters as seen from an observer at the Galactic center for the hemisphere containing S0-2. Degeneracy in the inclination angle for the other stars can not re-position the vectors in this hemisphere. The He I star plane of Levin & Beloborodov (2003) is shown as a 20° wide band. At the 2σ , deviation from an isotropic distribution is detected.